



# High-resolution CINE imaging of active guided knee motion using continuously acquired golden-angle radial MRI and rotary sensor information

Martin Aleksiev <sup>a,1</sup>, Martin Krämer <sup>a,b,\*1</sup>, Nicholas M. Brisson <sup>c</sup>, Marta B. Maggioni <sup>a</sup>, Georg N. Duda <sup>c</sup>, Jürgen R. Reichenbach <sup>a</sup>

<sup>a</sup> Medical Physics Group, Institute of Diagnostic and Interventional Radiology, Jena University Hospital, Friedrich Schiller University Jena, Germany

<sup>b</sup> Institute of Diagnostic and Interventional Radiology, Jena University Hospital, Friedrich Schiller University Jena, Germany

<sup>c</sup> Julius Wolff Institute, Berlin Institute of Health at Charité – Universitätsmedizin Berlin, Germany

## ARTICLE INFO

**Keywords:**  
Knee motion  
Radial MRI  
Golden-angle  
Real-time  
CINE

## ABSTRACT

To explore and extend on dynamic imaging of joint motion, an MRI-safe device guiding knee motion with an attached rotary encoder was used in MRI measurements of multiple knee flexion-extension cycles using radial gradient echo imaging with the golden-angle as azimuthal angle increment. Reproducibility of knee motion was investigated. Real-time and CINE mode anatomical images were reconstructed for different knee flexion angles by synchronizing the encoder information with the MRI data, and performing flexion angle selective gating across multiple motion cycles. When investigating the influence of the rotation angle window width on reconstructed CINE images, it was found that angle windows between 0.5° and 3° exhibited acceptable image sharpness without suffering from significant motion-induced blurring. Furthermore, due to flexible retrospective image reconstruction afforded by the radial golden-angle imaging, the number of motion cycles included in the reconstruction could be retrospectively reduced to investigate the corresponding influence of acquisition time on image quality. Finally, motion reproducibility between motion cycles and accuracy of the flexion angle selective gating were sufficient to acquire whole-knee 3D dynamic imaging with a retrospectively gated 3D cone UTE sequence.

## 1. Introduction

Musculoskeletal conditions are the highest contributor to global disability [1], comprising over 150 diagnoses that affect the locomotor system, including joints, bones, muscles, tendons and ligaments [2]. Such conditions can be acute (e.g., fractures, sprains, strains) or chronic (e.g., osteoarthritis, osteoporosis, sarcopenia), many of which are characterized by pain and reduced mobility [3]. Magnetic resonance imaging (MRI) is a leading modality in the assessment of the musculoskeletal system; however, it is conventionally performed in static configurations. Since joints are inherently dynamic, it is important to evaluate musculoskeletal conditions in the context of motion, as

abnormal joint motion can be implicated in the onset and progression of pain and pathology (e.g., osteoarthritis) due to altered contact mechanics between articulating surfaces and tissue straining (i.e., mechanical underloading or overloading) [4]. Importantly, information about tissue morphology and morphometry can be extracted and used to detect small but important changes associated with disease onset [5]. In addition, compositional changes such as elevated T<sub>2</sub> values may be used as markers of cartilage degeneration in knee osteoarthritis [6]. Two requirements must be met for morphological and compositional evaluation of knee joint tissues in the context of motion: (i) controlled and repeatable knee motion within the scanner bore and (ii) reconstruction techniques such as CINE [7] that allow for high-resolution imaging

**Abbreviations:** AW, Angle window; MC, Motion cycles; MRI, Magnetic resonance imaging; UTE, Ultra-short echo-time; ROI, Region of interest; SNR, Signal-to-noise ratio.

\* Corresponding author at: Medical Physics Group, IDIR, Jena University Hospital, Philosophenweg 3, D-07443 Jena, Germany.

E-mail addresses: [Martin.Kraemer@med.uni-jena.de](mailto:Martin.Kraemer@med.uni-jena.de) (M. Krämer), [nicholas.brisson@charite.de](mailto:nicholas.brisson@charite.de) (N.M. Brisson), [marta.maggioni@uni-jena.de](mailto:marta.maggioni@uni-jena.de) (M.B. Maggioni), [georg.duda@charite.de](mailto:georg.duda@charite.de) (G.N. Duda), [Juergen.Reichenbach@med.uni-jena.de](mailto:Juergen.Reichenbach@med.uni-jena.de) (J.R. Reichenbach).

<sup>1</sup> Both authors contributed equally.

<https://doi.org/10.1016/j.mri.2022.06.015>

Received 25 February 2022; Received in revised form 13 June 2022; Accepted 23 June 2022

Available online 29 June 2022

0730-725X/© 2022 The Author(s). Published by Elsevier Inc. This is an open access article under the CC BY license (<http://creativecommons.org/licenses/by/4.0/>).

during joint motion at speeds that are physiologically relevant. An MRI-safe device for guided knee motion can help achieve both of these goals.

To facilitate repeatable knee motion in the sagittal plane during dynamic MRI, previous studies have used vertical coil holders [8–10] and leg braces with ankle support [8,10–14] to restrict unwanted out-of-plane limb displacement. Prior work presented CINE knee images from 2D dynamic data with spatial resolution between 0.7 and 1.17 mm<sup>2</sup> acquired with Cartesian sequences [8–13,15–17]. To synchronize the joint motion with data acquisition and reconstruction, these studies used optical sensors and transducers [4,5,10,11], a plethysmograph [10,11], or a pseudo-electrocardiogram via a pneumatic pressure transducer [12,13,17] to mark a position in the motion cycle that acted as a trigger for the MRI acquisition. One potential problem with such an approach is inconsistent joint motion throughout the motion cycles. For example, knee displacement between multiple motion cycles could result in capturing the leg at different positions in space, resulting in images suffering from motion artifacts when using sequentially sampled Cartesian MRI sequences [8].

A better approach could be the use of continuously acquired real-time sensor information of the knee flexion angle for synchronization with the MRI data and CINE image reconstruction, as demonstrated by Kaiser et al. [14]. Here, we extend the implementation of such an approach by combining continuously acquired radial golden-angle [18] MRI data with angular sensor information to retrospectively reconstruct CINE images of the knee, allowing the acquisition of high-resolution 2D and 3D UTE [19] whole-knee images during knee flexion and extension.

## 2. Methods

MRI measurements were performed on five healthy volunteers (aged between 22 and 37 years, body mass between 55 and 90 kg) using a clinical 3 T Siemens Prisma fit scanner. Volunteers had no known musculoskeletal conditions and gave written informed consent in accordance with the guidelines set out by the institutional ethics committee.

Knee motion was guided using a previously reported MRI-safe device, which was supported by the patient table and inner railings of the scanner bore (Fig. 1) [20]. The baseplate of the device has an opening through which the leg can move up and down, allowing for ~40° of knee flexion within the bore [20]. A fiber optic position sensor (MR338-Y10C10, Micronor, 155 Camarillo, CA, USA), which measures the absolute angle from 0° to 360° with a resolution of 0.025°, was attached to the device. The sensor continuously measured the angular displacement of the leg support (to which the lower leg is secured) as it rotates during knee flexion and extension. During measurements, volunteers were positioned supine on the device. The knee of interest was positioned so that its axis of rotation was aligned with that of the device, and was imaged by positioning two flexible coils around the knee, one anteriorly and the other posteriorly (Variety, NORAS MRI products GmbH, Höchberg, Germany). The thigh was fastened upon a wedge positioner, and the lower leg was fastened to the ankle rest approximately 2 cm proximal to the malleoli using Velcro straps. Volunteers performed knee flexion-extension cycles to the beat of a metronome at speeds ranging

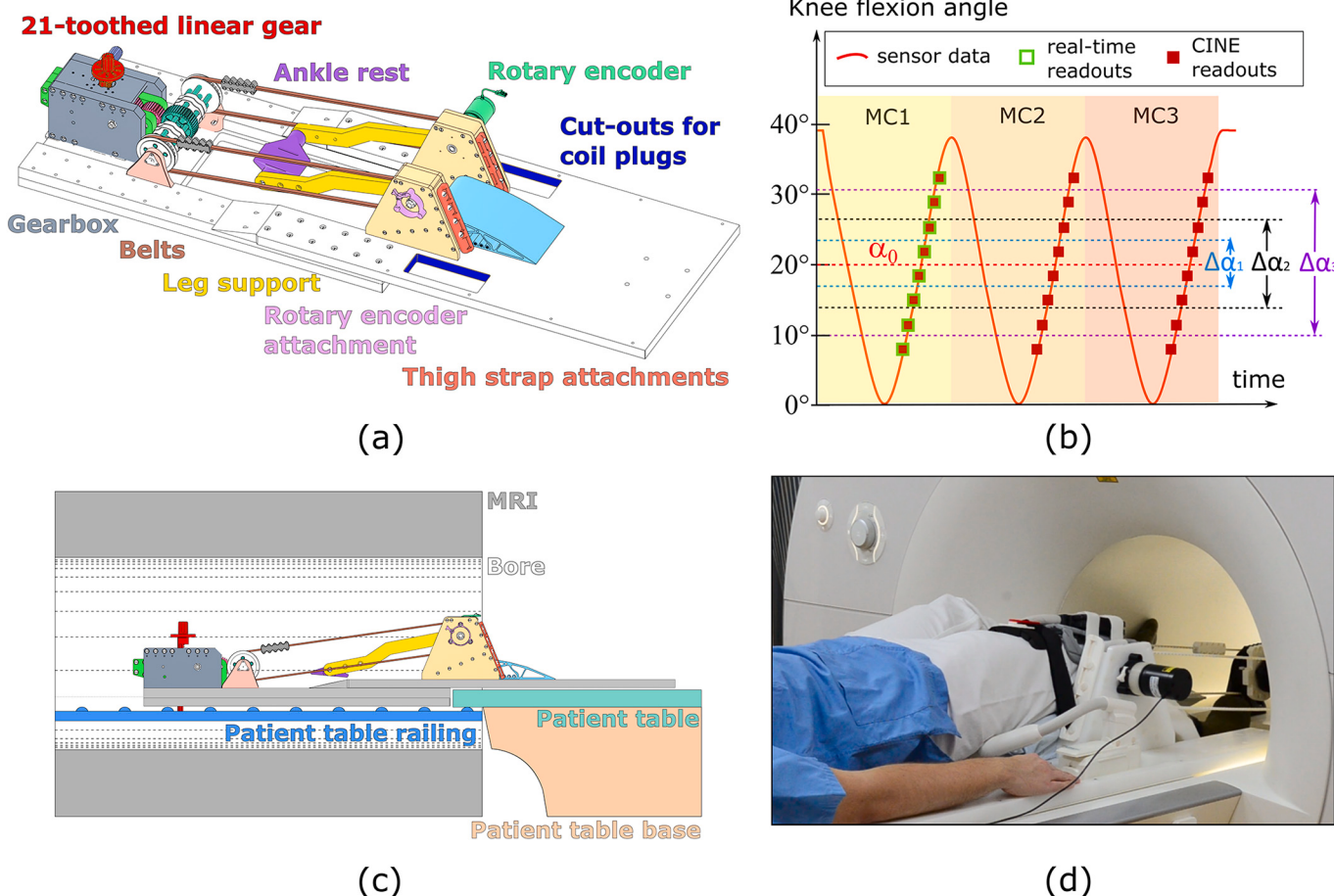


**Fig. 1.** (a) Depiction of the knee motion device with labelled components. Weight plates can be added to the device to load the leg, allowing for more physiologically relevant conditions. (b) Readouts for a specified angle  $\alpha_0$  and angle windows  $\Delta\alpha_1$ ,  $\Delta\alpha_2$  and  $\Delta\alpha_3$  during knee flexion-extension for 3 motion cycles (MC). Only the readouts outlined in green would be used for real-time reconstruction, while all readouts in red would be used for CINE reconstruction. (c) Side view depicting how the device fits on top of the patient table and inner bore railing. (d) Photograph of a patient positioned in the device near the bore opening. (For interpretation of the references to colour in this figure legend, the reader is referred to the web version of this article.)

between 7.5 and 30 cycles/min. A video showing an example of a subject performing supine and prone knee motion protocols using the device is available as open access supplementary material [20].

Synchronization of knee motion with the MRI data was performed by simultaneously acquiring a trigger at the start of each sequence repetition together with the continuously acquired angular encoder data. One sequence repetition was defined as the acquisition of the number of readouts required to fully sample k-space. Based on the triggers, the number of readouts per sequence repetition, and the encoder data, corresponding timestamps and knee flexion angles were assigned to individual readouts. For k-space sampling, a radial golden-angle gradient-echo FLASH sequence was used [7,18,21], which is more robust against motion artifacts than Cartesian sequences and offers flexibility for image reconstruction. The use of radial golden-angle temporal ordering enabled image reconstruction from readout windows of arbitrary width and temporal position, and from any combination of windows (i.e., using readouts from two separate windows that do not overlap or are contiguous) [18]. For retrospective real-time and CINE reconstruction, readouts were binned into knee flexion angle windows with a specified range, allowing image reconstruction at any known angle of the knee. For real-time reconstruction, readouts acquired during a single flexion-extension cycle were used; whereas for CINE reconstruction, readouts acquired during multiple motion cycles were used (Fig. 1). Due to physiological differences in knee tissue morphology and morphometry between movement types, only readouts from either flexion or extension were used for image reconstruction. All image reconstruction and data analysis were performed offline using MATLAB (version 2019a, The MathWorks, Inc., Natick, Massachusetts, USA). Re-gridding of the radial data was performed using iterative sampling density compensation and an optimized gridding kernel [22].

To investigate the reproducibility of the dynamic MRI measurements and the consistency of the knee motion achievable using said device, a single transverse slice of the knee through the femur was acquired for each volunteer using 200 sequence repetitions of a radial golden-angle FLASH sequence. Acquisition parameters were:  $144 \times 144$  matrix,  $220 \times 220 \text{ mm}^2$  field of view,  $1.5 \times 1.5 \text{ mm}^2$  spatial resolution, 4.8 mm slice thickness,  $10^\circ$  flip angle, 2.4 ms echo time, 5.1 ms repetition time, with acquisition duration of 3:51 min and knee motion speed of 7.5 cycles/min. The motion speed of 7.5 cycles/min was chosen to collect sufficient readouts for real-time reconstruction so that the femur could be identified within each flexion-extension cycle and a region of interest (ROI) could be drawn around it. Real-time images were reconstructed at the  $25^\circ$  position with a  $2^\circ$  window from each of the 28 flexion-extension

cycles actively performed by the volunteers for each of the five MRI measurements. A region of interest of the femur was defined in the first frame of a measurement and rigidly translated to match the femur position in the remaining 27 frames (Fig. 2a). Subsequently, the frame-to-frame shift of the femur ROI in the x- and y-directions was determined based on the ROI centroid.

For CINE reconstruction, a single 2D sagittal slice of the knee was repetitively acquired with 65 sequence repetitions of a radial golden-angle FLASH sequence with the following acquisition parameters:  $320 \times 320$  matrix size,  $210 \times 210 \text{ mm}^2$  field of view,  $0.66 \times 0.66 \text{ mm}^2$  spatial resolution, 3 mm slice thickness,  $10^\circ$  flip angle, 2.4 ms echo time, 7.0 ms repetition time, total acquisition duration of 3:48 min and knee motion speed of 7.5 cycles/min. The relatively slow motion speed was chosen to enable real-time reconstructed images that could be compared with CINE images. For comparison, real-time and CINE images were reconstructed at four different angles of  $6^\circ$ ,  $14^\circ$ ,  $22^\circ$  and  $30^\circ$  using a  $2^\circ$  window. Reconstructing images with a larger angle window would include more radial readouts acquired when the knee is in different positions, thus reducing the angle precision. To examine the effects of the window on angle precision, CINE images were reconstructed with angle windows of  $0.25^\circ$ ,  $0.5^\circ$ ,  $1^\circ$ ,  $2^\circ$ ,  $3^\circ$ ,  $4^\circ$ ,  $6^\circ$  and  $8^\circ$  for a knee flexion angle of  $22^\circ$ . A 1D profile line was drawn perpendicular to the tibia at the same position for each of the aforementioned images to observe how the signal intensity along the profile line changed for the different angle windows.

An important aspect of CINE imaging of the knee is the dependency of the reconstructed images on the number of motion cycles and the resulting scan time, features that should be minimized to improve comfort, reduce muscular fatigue and enable future studies in patient populations. To determine the extent to which scan time could be reduced so that CINE images did not visually suffer substantially from undersampling artifacts, a single 2D sagittal slice of the knee was acquired for knee motion at a faster speed of 30 cycles/min, and with the following sequence parameters:  $144 \times 144$  matrix size,  $220 \times 220 \text{ mm}^2$  field of view,  $1.5 \times 1.5 \text{ mm}^2$  spatial resolution, 4.8 mm slice thickness,  $10^\circ$  flip angle, 2.4 ms echo time, 5.6 ms repetition time with a total acquisition duration of 3:22 min. CINE images were reconstructed for an angle of  $15^\circ$  with a  $2^\circ$  window using readouts from 10, 30, 45 and 101 flexion-extension cycles for comparison.

For 3D dynamic imaging and visualization of tissues with short  $T_2$  relaxation times such as tendons and ligaments, a 3D scan of the whole knee was acquired for knee motion at a speed of 23 cycles/min using a radial 3D cone UTE sequence [19,23,24] with segmentation factor 96

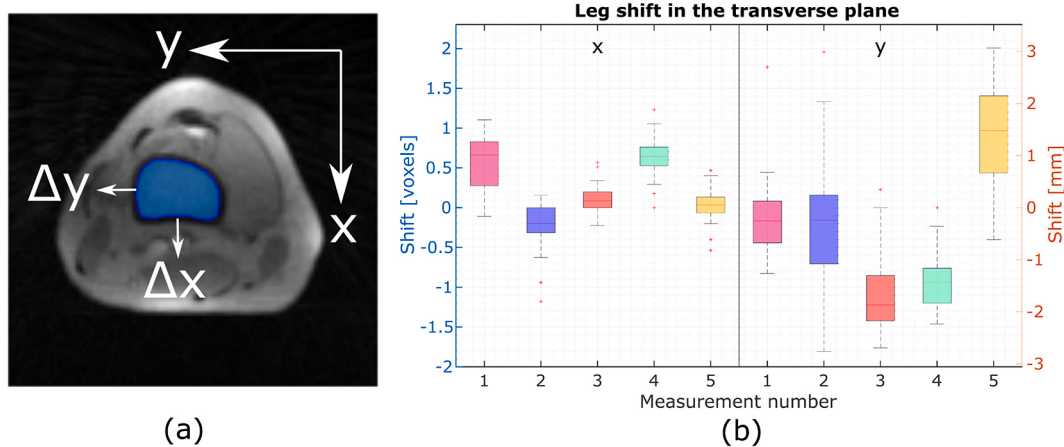


**Fig. 2.** (a) Real-time reconstructed image of a transverse slice through the femur with a corresponding ROI drawn in blue. Copying the ROI to another frame and aligning it with the femur using rigid operations, the ROI centroid exhibits shifts of  $\Delta x$  and  $\Delta y$  in the x-direction (anterior/posterior) and y-direction (lateral/medial), respectively. (b) Boxplots of the shifts resulting from the 28 frames for each volunteer. The average shift across all measurements and volunteers was 0.26 voxels (0.39 mm) for the x-direction and 0.56 voxels (0.84 mm) for the y-direction. (For interpretation of the references to colour in this figure legend, the reader is referred to the web version of this article.)

and whole-knee coverage. With k-space segmentation, acquisition of one segment took 0.17 s, meaning that one transit of 3D k-space was much faster than the duration of one flexion-extension cycle, resulting in a more uniform distribution of readouts after retrospective gating. Parameters were:  $112 \times 94 \times 18$  matrix size,  $180 \times 150 \times 72$  mm $^3$  field of view,  $1.6 \times 1.6 \times 4$  mm $^3$  spatial resolution,  $4^\circ$  flip angle, 0.03 ms echo time, 1.5 ms repetition time with a total acquisition duration of 4:57 min. CINE images were reconstructed using a  $3^\circ$  window. This wider angle window was used to include more readouts in the reconstruction of dynamic 3D k-spaces and to reduce the effects of undersampling.

### 3. Results

Femur translation in x- and y- directions during repeated motion relative to the first frame are shown in Fig. 2b. Although some measurements showed a translation of the femur of up to 1.5 voxels in the x-direction and 3 voxels in the y-direction, the average femur displacement across all five measurements was 0.26 and 0.56 voxels (0.39 and 0.84 mm), respectively.

Real-time and CINE reconstructed images for four knee angles are shown in Fig. 3. While the real-time images suffered from streaking artifacts and blurring, the CINE images appeared visually sharper and free of streaking and undersampling artifacts. In addition, the real-time

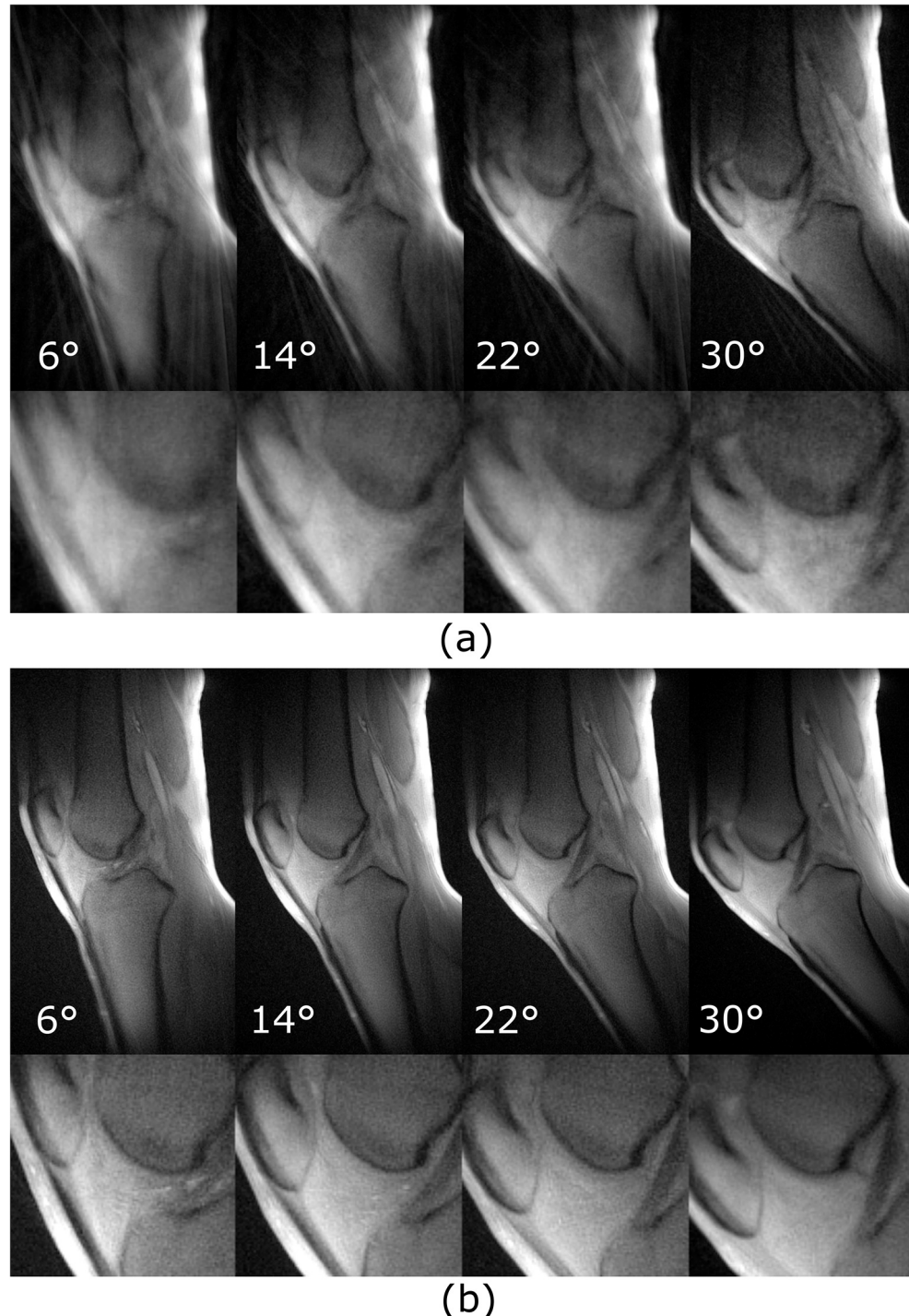


**Fig. 3.** (a) Real-time and (b) CINE images (with zoomed-in versions below) reconstructed for 4 different angles with a  $2^\circ$  window. The images in (a) were reconstructed from readouts during a single motion cycle. Inconsistencies in the knee motion such as speed and range of motion resulted in some images having less undersampling artifacts than others. The images in (b) are visually more consistent with respect to undersampling artifacts because they were reconstructed from multiple motion cycles, reducing the effects of undesired motion.

images for different angles appeared to be inconsistent with respect to undersampling artifacts (e.g., the 6° and 30° real-time images), likely due to inconsistency in knee motion speed during a given motion cycle despite use of the metronome. The k-space sampling percentages for the 6°, 14°, 22° and 30° real-time images shown in Fig. 3 were 5.4%, 9.0%, 8.4% and 17.3%, respectively. As the knee motion speed increased, fewer radial readouts were acquired for a given angle, resulting in a smaller k-space sampling percentage compared to slower knee motions. In comparison, the k-space sampling percentages for the 6°, 14°, 22° and 30° CINE images were 83.7%, 89.0%, 96.4% and 100%, respectively. A video showing all reconstructed real-time and CINE frames is available (Supplementary Video 1). CINE images for eight different angle windows are displayed in Fig. 4, where images with a smaller window appeared to suffer from undersampling artifacts (i.e., streaking and blurring) and increased noise, while images with a larger window appeared blurred due to poor definition of the knee angle. These results suggest that there is an optimal range of angle windows that includes enough readouts to avoid undersampling artifacts while not substantially sacrificing knee angle precision.

The observation that larger angle windows caused blurring was further confirmed by a profile through the tibia in Fig. 5, which showed broadening and signal reduction in the skin-to-tendon transition region for angle windows of 6° and greater. Specifically, broadening between the 10 and 90 mm distance marks along the profile line was evident at windows greater than 2°. This again suggests that there is an optimal/acceptable range of angle windows that can be used for image reconstruction, namely windows of 1° and 2°.

Fig. 6 shows CINE images for a 30 cycles/min measurement, reconstructed with readouts acquired during 10, 30, 45 and 101 knee flexion-extension cycles. The images demonstrate that reconstruction of CINE images from as little as 60 s of knee motion (such as image C30)

was feasible and visually comparable to images reconstructed from 202 s of knee motion. This was further supported by the k-space sampling percentages of the C10, C30, C45 and C101 images, which were 31.4%, 70.4%, 84.1% and 96.9%, respectively.

Fig. 7 shows CINE images of a 3D UTE scan for different slices demonstrating dynamic whole-knee imaging. Due to the higher number of readouts required to fill the 3D k-space, the k-space of the images shown in the figure are 52% sampled. Nevertheless, complete coverage of the knee was achieved, including all structures of the knee. A video showing reconstructed CINE frames for different slices and knee angles is available (Supplementary Video 2).

#### 4. Discussion

Dynamic MRI measurements of the knee using an MRI-safe device for guided motion with a rotary encoder allowed CINE reconstruction of images with the potential for morphological and compositional evaluation of knee tissues. Using the referred knee device [20], the average femur displacement across all five measurements was less than 1 voxel in the x- and y-directions. Consequently, undesired leg displacement between motion cycles should not cause significant blurring and should have little effect on image sharpness. When using continuously acquired golden-angle radial data for retrospective CINE reconstruction, it is important to choose the angle window carefully, as small windows can result in undersampling artifacts and loss of signal-to-noise ratio (SNR), while larger windows can result in blurring due to the actual motion being studied. While a smaller angle window was advantageous for obtaining sharp images best suited for morphological evaluation, a larger angle window allowed for shorter measurement time by increasing the SNR – ultimately leading to a trade-off between knee angle certainty and the number of readouts for reconstruction. Due to

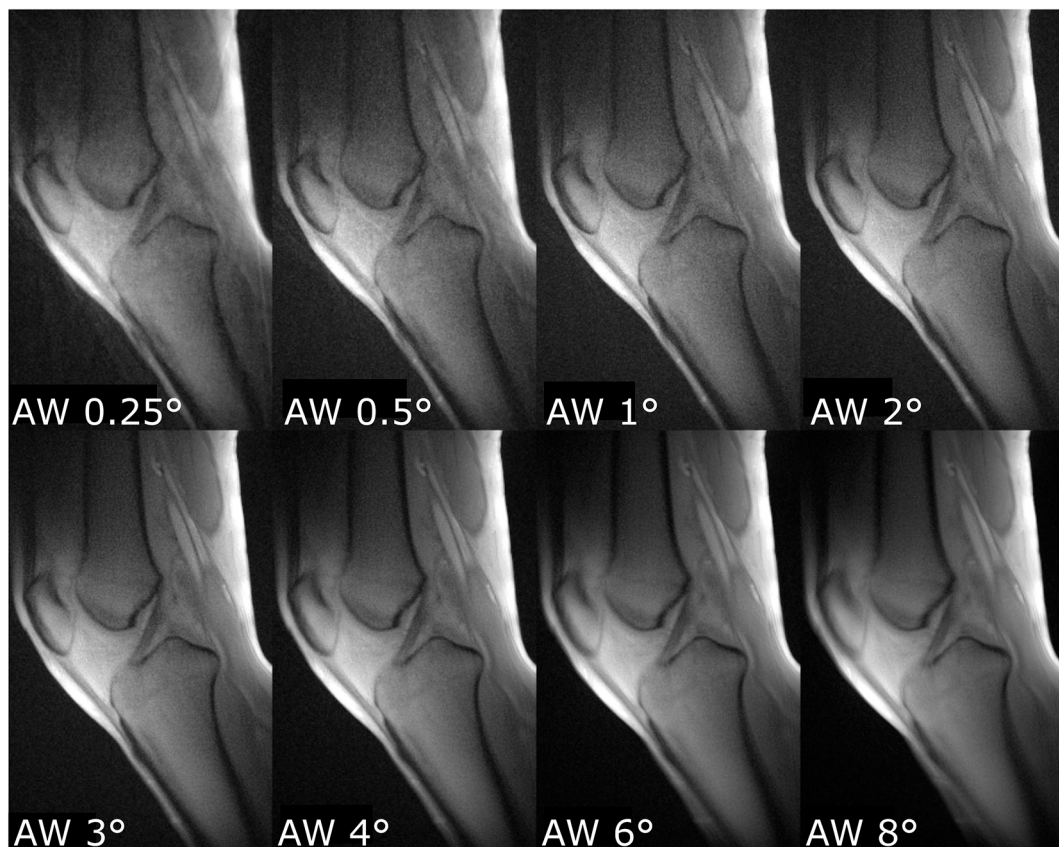


**Fig. 4.** CINE images reconstructed for 8 different angle windows (AW). Increasing the angle window led to more readouts being included in image reconstruction, thereby increasing SNR but reducing angle precision and resulting in blurred images (see Fig. 5).

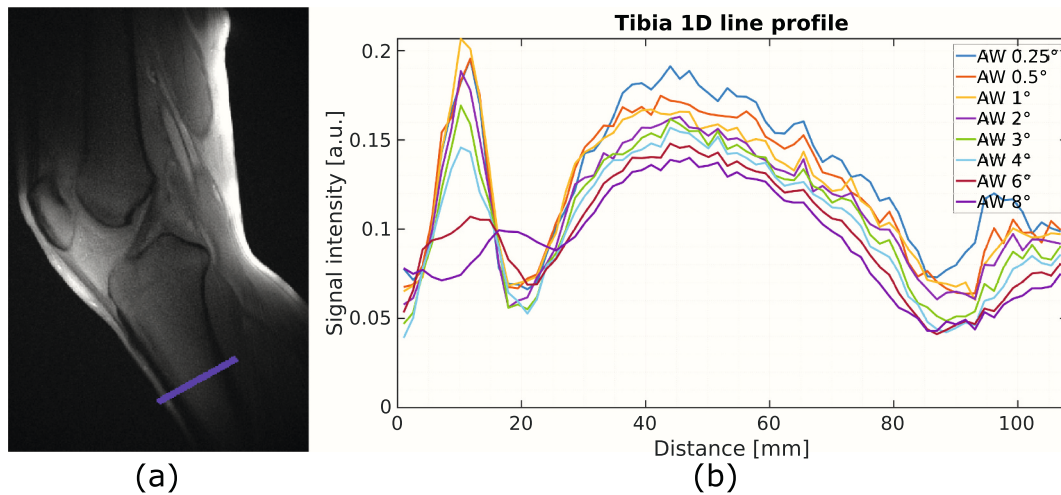


**Fig. 5.** (a) CINE image of a sagittal slice with a 1D profile line (in blue) drawn perpendicular to and through the tibia. (b) The same line was copied to all images from Fig. 4, and the signal intensity along the line was plotted for each angle window. Larger angle windows (i.e., 6° and greater) resulted in significant broadening and signal reduction between the 10 and 90 mm distance marks along the profile line. (For interpretation of the references to colour in this figure legend, the reader is referred to the web version of this article.)

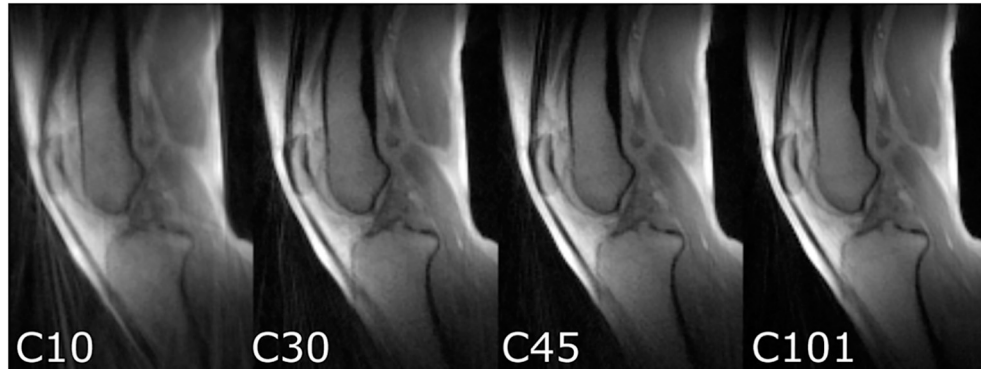


**Fig. 6.** CINE images reconstructed from a 30 cycles/min measurement using readouts acquired during 10, 30, 45 and 101 cycles (C) of knee flexion and extension, corresponding to 20, 60, 90 and 202 s of motion, respectively. The images suggest that reconstruction of CINE images from as little as 60 s of knee motion (i.e., image C30) is feasible and visually comparable to images reconstructed from 202 s of knee motion.

the golden-angle radial acquisition, this trade-off can only be adapted during image reconstruction. Overall, a range of angle windows between 0.5° and 3° is proposed for yielding acceptable image sharpness without significant motion-induced blurring.

Compared with previous work focusing on 2D imaging [8–13,15–17], image resolution and severity of motion artifacts were improved, likely due to the use of a rotary position sensor to continuously gate the CINE reconstruction and the radial golden-angle acquisition. The optical triggers [8,9,15,16], plethysmograph [10,11] and pseudo-electrocardiogram [12,13,17] of previous work used only one trigger for each motion cycle. Such triggers do not account for motion variability and thus can lead to artifacts in gated CINE images [8], especially when Cartesian sequences are used. In comparison, the additional information provided by the position sensor enabled the recording of the time and knee angle at which each individual readout was acquired. In combination with the radial golden-angle sequence, this renders the retrospectively reconstructed CINE images insensitive to inconsistent knee motion speed and thus more flexible with respect to gating [18]. The use of a sturdy and specialized knee motion device [20] is likely another reason for the improved image quality.

The maximum knee flexion-extension speed of 30 cycles/min used in this study was comparable to speeds previously reported [8–13,15–17]. The 7.5 cycles/min motion speed was used for reconstructing real-time

images, which would have had too few readouts if the speed had been faster. The 23 cycles/min motion speed was used during the 3D UTE scan to improve volunteer comfort during the longer acquisition duration.

Dynamic MRI measurements using 3D UTE acquisition enabled 3D CINE reconstruction of knee data with ultra-short TE that included tendon and ligament signal. The only known similar work by Kaiser et al. used a more conventional TE of 1.4 ms [14]. Furthermore, in the study of Kaiser et al. an angle window of approximately 1.2° was used, resulting in highly undersampled 3D datasets. Based on the stability analysis we have performed beforehand, an angle window of 3° could be chosen for reconstruction of dynamic 3D UTE data, including more readouts, and thus reaching a k-space sampling of slightly above 50%. This effectively decreased the severity of image artifacts without significant blurring and improved image sharpness. To further reduce undersampling, longer measurement times could be used so that more readouts are acquired overall. However, the increase in scan time could be a potential drawback for practical applications, especially in subjects with knee injuries or pathologies who may suffer from pain or other symptoms. Another option would be to acquire 3D scans using a radial stack of stars trajectory [25], which would also capture the entire knee and allow use of the radial golden angle. This could result in improved k-space sampling compared to the 3D UTE sequence but at the cost of

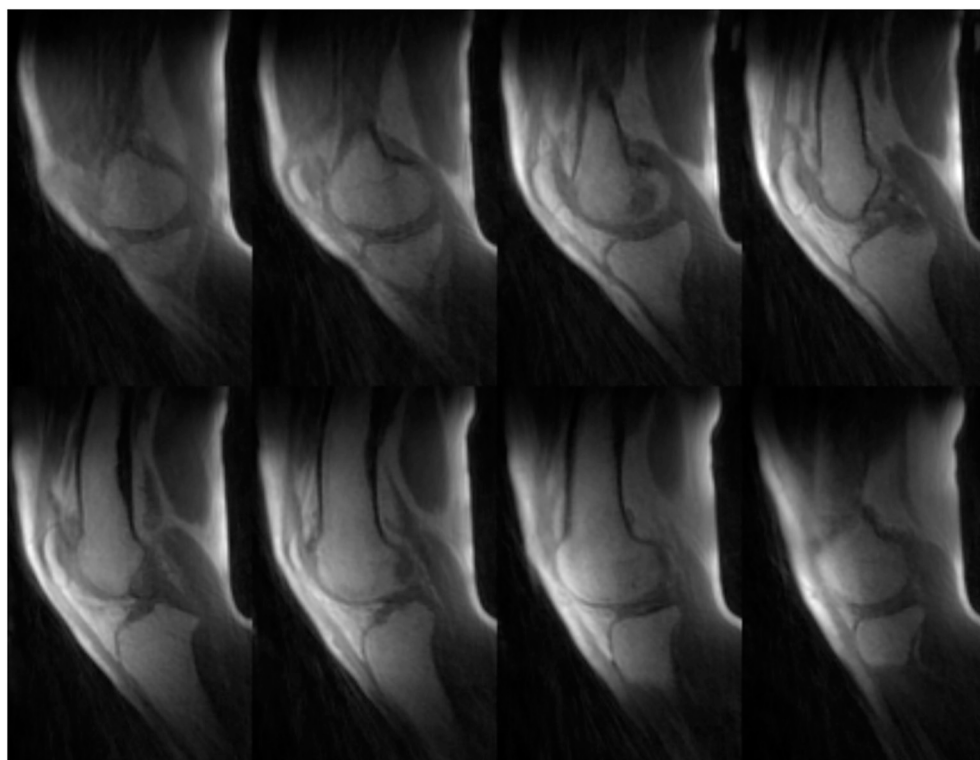


**Fig. 7.** CINE images of every other slice between slice numbers 25 and 39 (out of 55) from a 3D UTE scan for a single knee angle of 25°, demonstrating larger spatial coverage of the whole knee for dynamic MRI.

increased sensitivity against motion artifacts due to the Cartesian encoding in z-direction. Alternatively, state-of-the-art acceleration algorithms [26,27] could be applied to the dynamic 3D UTE sequence to further improve resolution and image quality or reduce scan time. Nevertheless, direct acquisition of dynamic 3D CINE images covering the entire knee has the potential to eliminate the need for complex slice-to-volume registration techniques [16,28].

## 5. Conclusion

In conclusion, we have demonstrated that the combination of continuously acquired angular sensor data with a radial golden-angle sampling is advantageous for dynamic CINE imaging of the knee. The presented acquisition and gating scheme allows high flexibility in data reconstruction and enables not only high-resolution dynamic 2D imaging but also dynamic 3D imaging of the whole knee. Using this setup, there is great potential for investigating *in vivo* knee tissue deformations in response to different knee motion and loading conditions in a time-resolved, detailed and systematic manner in future MRI studies. Such information will be invaluable for elucidating the role of joint motion and loading in the development and worsening of musculoskeletal conditions.

Supplementary data to this article can be found online at <https://doi.org/10.1016/j.mri.2022.06.015>.

## Funding sources

This work was supported by the German Research Foundation (DFG - Deutsche Forschungsgemeinschaft, DU 298/25-1, RE 1123/22-1, KR 4783/2-1, BR 6698/1-1). Further support is acknowledged from the Competence Center for Interdisciplinary Prevention (KIP - Kompetenzzentrum für Interdisziplinäre Prävention) at the Friedrich Schiller University Jena and the German Professional Association for the Food and Hospitality Industry (BGN - Berufsgenossenschaft Nahrungsmittel

und Gastgewerbe). The funding sources had no influence on the study design, the collection, analysis and interpretation of the data, the writing of the manuscript, or the decision to submit the article for publication.

## CRediT authorship contribution statement

**Martin Aleksiev:** Methodology, Software, Investigation, Writing – original draft, Visualization, Data curation. **Martin Krämer:** Conceptualization, Methodology, Investigation, Writing – review & editing, Visualization, Supervision, Data curation. **Nicholas M. Brisson:** Conceptualization, Validation, Writing – review & editing. **Marta B. Maggioni:** Investigation, Resources, Data curation. **Georg N. Duda:** Conceptualization, Writing – review & editing, Supervision. **Jürgen R. Reichenbach:** Conceptualization, Writing – review & editing, Supervision.

## Acknowledgments

The authors would like to thank the Research Workshop at the Charité – Universitätsmedizin Berlin for the construction of the MRI knee motion/loading device and the study volunteers.

## References

- [1] James SL, Abate D, Abate KH, Abay SM, Abbafati C, Abbasi N, et al. Global, regional, and national incidence, prevalence, and years lived with disability for 354 diseases and injuries for 195 countries and territories, 1990–2017: a systematic analysis for the global burden of disease study 2017. Lancet 2018;392(10159): 1789–858. [https://doi.org/10.1016/S0140-6736\(18\)32279-7](https://doi.org/10.1016/S0140-6736(18)32279-7).
- [2] World Health Organization, editor. ICD-11: International classification of diseases (11th revision). Retrieved from, <https://icd.who.int/>; 2022.
- [3] Blyth FM, Briggs AM, Schneider CH, Hoy DG, March LM. The global burden of musculoskeletal pain—where to from here? Am J Public Health 2019;109(1):35–40. <https://doi.org/10.2105/AJPH.2018.304747>.

- [4] Andriacchi TP, Koo S, Scanlan SF. Gait mechanics influence healthy cartilage morphology and osteoarthritis of the knee. *J Bone Joint Surg Am* 2009;91(Suppl. 1):95–101. <https://doi.org/10.2106/JBJS.H.01408>.
- [5] Roemer FW, Eckstein F, Guermazi A. Magnetic resonance Imaging-based Semiquantitative and quantitative assessment in osteoarthritis. *Rheum Dis Clin North Am* 2009;35(3):521–55. <https://doi.org/10.1016/j.rdc.2009.08.006>.
- [6] Li X, Benjamin Ma C, Link TM, Castillo D-D, Blumenkrantz G, Lozano J, et al. In vivo T1ρ and T2 mapping of articular cartilage in osteoarthritis of the knee using 3T MRI. *Osteoarthr Cartil* 2007;15(7):789–97. <https://doi.org/10.1016/j.joca.2007.01.011>.
- [7] Krämer M, Herrmann K-H, Biermann J, Reichenbach JR. Retrospective reconstruction of cardiac cine images from Golden-ratio radial MRI using one-dimensional navigators: 1D navigator Golden-ratio radial cine Imaging. *J Magn Reson Imaging* 2014;40(2):413–22. <https://doi.org/10.1002/jmri.24364>.
- [8] Sheehan FT, Zajac FE, Drace JE. Using cine phase contrast magnetic resonance imaging to non-invasively study in vivo knee dynamics. *J Biomech* 1997;31(1):21–6. [https://doi.org/10.1016/S0021-9290\(97\)00109-7](https://doi.org/10.1016/S0021-9290(97)00109-7).
- [9] Carlson VR, Boden BP, Sheehan FT. Patellofemoral kinematics and tibial tuberosity-trochlear groove distances in female adolescents with patellofemoral pain. *Am J Sports Med* 2017;45(5):1102–9. <https://doi.org/10.1177/0363546516679139>.
- [10] Westphal CJ, Schmitz A, Reeder SB, Thelen DG. Load-dependent variations in knee kinematics measured with dynamic MRI. *J Biomech* 2013;46(12):2045–52. <https://doi.org/10.1016/j.jbiomech.2013.05.027>.
- [11] Silder A, Westphal CJ, Thelen DG. A magnetic resonance-compatible loading device for dynamically Imaging shortening and lengthening muscle contraction mechanics. *J Med Devices* 2009;3(3):034504. <https://doi.org/10.1115/1.3212559>.
- [12] Broßmann J, Mühlé C, Schröder C, Melchert UH, Büll CC, Spielmann RP, et al. Patellar tracking patterns during active and passive knee extension: evaluation with motion-triggered cine MR imaging. *Radiology* 1993;187(1):205–12. <https://doi.org/10.1148/radiology.187.1.8451415>.
- [13] Broßmann J, Mühlé C, Büll CC, Schröder C, Melchert UH, Zieplies J, et al. Evaluation of patellar tracking in patients with suspected patellar malalignment: cine MR imaging vs arthroscopy. *Am J Roentgenol* 1994;162(2):361–7. <https://doi.org/10.2214/ajr.162.2.8310928>.
- [14] Kaiser J, Vignos MF, Liu F, Kijowski R, Thelen DG. American Society of Biomechanics Clinical Biomechanics Award 2015: MRI assessments of cartilage mechanics, morphology and composition following reconstruction of the anterior cruciate ligament. *Clin Biomech* 2016;34:38–44. <https://doi.org/10.1016/j.climbiomech.2016.03.007>.
- [15] Barrance PJ, Williams GN, Snyder-Mackler L, Buchanan TS. Altered knee kinematics in ACL-deficient non-copers: a comparison using dynamic MRI. *J Orthop Res* 2006;24(2):132–40. <https://doi.org/10.1002/jor.20016>.
- [16] Borotikar BS, Sipprell WH, Wible EE, Sheehan FT. A methodology to accurately quantify patellofemoral cartilage contact kinematics by combining 3D image shape registration and cine-PC MRI velocity data. *J Biomech* 2012;45(6):1117–22. <https://doi.org/10.1016/j.jbiomech.2011.12.025>.
- [17] Broßmann J, Mühlé C, Büll CC, Zieplies J, Melchert UH, Brinkmann G, et al. Cine MR imaging before and after realignment surgery for patellar maltracking ? Comparison with axial radiographs. *Skeletal Radiol* [Internet] 1995;24(3). <https://doi.org/10.1007/BF00228921>.
- [18] Winkelmann S, Schaeffter T, Koehler T, Eggens H, Doessl O. An optimal radial profile order based on the Golden ratio for time-resolved MRI. *IEEE Trans Med Imaging* 2007;26(1):68–76. <https://doi.org/10.1109/TMI.2006.885337>.
- [19] Herrmann K-H, Krämer M, Reichenbach JR. Time efficient 3D radial UTE sampling with fully automatic delay compensation on a clinical 3T MR scanner. Fan X, editor. *PLoS One* 2016;11(3):e0150371. <https://doi.org/10.1371/journal.pone.0150371>.
- [20] Brisson NM, Krämer M, Krahl LAN, Schill A, Duda GN, Reichenbach JR. A novel multipurpose device for guided knee motion and loading during dynamic magnetic resonance imaging. *Z Für. Med Phys* 2022. <https://doi.org/10.1016/j.zemedi.2021.12.002>. S093938892100115X.
- [21] Haase A, Frahm J, Matthaei D. Flash imaging rapid nmr imaging using low flip-angle pulses. *J Magn Reson* 1986;67:258–66. [https://doi.org/10.1016/0022-2364\(86\)90433-6](https://doi.org/10.1016/0022-2364(86)90433-6).
- [22] Zwart NR, Johnson KO, Pipe JG. Efficient sample density estimation by combining gridding and an optimized kernel. *Magn Reson Med* 2012;67(3):701–10. <https://doi.org/10.1002/mrm.23041>.
- [23] Krämer M, Maggioni MB, Brisson NM, Zachow S, Teichgräber U, Duda GN, et al. T1 and T2<sup>\*</sup> mapping of the human quadriceps and patellar tendons using ultra-short echo-time (UTE) imaging and bivariate relaxation parameter-based volumetric visualization. *Magn Reson Imaging* 2019;63:29–36. <https://doi.org/10.1016/j.mri.2019.07.015>.
- [24] Renz DM, Herrmann K-H, Kraemer M, Boettcher J, Waginger M, Krueger P-C, et al. Ultrashort echo time MRI of the lung in children and adolescents: comparison with non-enhanced computed tomography and standard post-contrast T1w MRI sequences. *Eur Radiol* [Internet] 2021. <https://doi.org/10.1007/s00330-021-08236-7>.
- [25] Kecskemeti S, Johnson K, Wu Y, Mistretta C, Turski P, Wieben O. High resolution three-dimensional cine phase contrast MRI of small intracranial aneurysms using a stack of stars k-space trajectory. *J Magn Reson Imaging* 2012;35(3):518–27. <https://doi.org/10.1002/jmri.23501>.
- [26] Lustig M, Donoho D, Pauly JM. Sparse MRI: the application of compressed sensing for rapid MR imaging. *Magn Reson Med* 2007;58(6):1182–95. <https://doi.org/10.1002/mrm.21391>.
- [27] Wright KL, Hamilton JI, Griswold MA, Gulani V, Seiberlich N. Non-Cartesian parallel imaging reconstruction: non-Cartesian parallel Imaging. *J Magn Reson Imaging* 2014;40(5):1022–40. <https://doi.org/10.1002/jmri.24521>.
- [28] Lin C-C, Zhang S, Frahm J, Lu T-W, Hsu C-Y, Shih T-F. A slice-to-volume registration method based on real-time magnetic resonance imaging for measuring three-dimensional kinematics of the knee: slice-to-volume registration using real-time MRI. *Med Phys* 2013;40(10):102302. <https://doi.org/10.1118/1.4820369>.